SCIREA Journal of Mathematics

http://www.scirea.org/journal/Mathematics

June 4, 2019

Volume 4, Issue 3, June 2019

Convective heat transfer of Ferrofluids over a Flat Plate with Slip Condition and Radiation

Anika Ferdous[1] , Tania S. Khaleque[2,*]

[1]Department of Mathematics and Natural Sciences, BRAC University, 66 Mohakhali, Dhaka-1212, Bangladesh, anika.ferdous@bracu.ac.bd

[2]Department of Applied Mathematics, University of Dhaka, Dhaka-1000, Bangladesh; tania.khaleque@du.ac.bd

*Correspondence: tania.khaleque@du.ac.bd; Tel.: +88-019210-82872

Abstract

The present study considered the thermal convection of ferrofluids along a flat plate subject to uniform heat flux and slip velocity in the presence of radiation with a magnetic field applied in the transverse direction. Two different types of ferrofluids are considered: one magnetic nanoparticle (Fe_3O_4) and one non-magnetic nanoparticle (TiO_2) that are incorporated within two different kinds of base fluids, water and kerosene oil. Numerical solutions are obtained using a finite difference scheme named Keller-Box method for each mixture of base fluids with Fe_3O_4 and TiO_2 for the variations of volume fraction, magnetic field, velocity slip, radiation and suction and the results are compared with the available data. The effects of different parameters are presented graphically and discussed.The variation of skin friction coefficient and heat transfer rate, i.e. the Nusselt Number are also shown in tabular form.

Keywords: Ferrofluids, Keller-Box method, velocity slip, skin friction coefficient, heat transfer rate.

1. Introduction

Nanoparticles with the size range under 100 nm in heat transfer fluid are commonly known as nanofluids. Choi [1] used the term nanofluids for the very first time and studied its thermal properties. Then it has been used byXuan and Li [2], Tiwari and Das [3], Ahmad *et al.* [4]and many other researchers. Application of nanoparticles provides an effective way of improving heat transfer characteristics of fluids. Among different kinds of researches on nanofluids, some of the studies have been focused on the nanofluids prepared by dispersing magnetic nanoparticles (3-15 nm) in a carrier liquid. These are called *ferrofluid*s. Tangthieng*et al.* [5] described the enhancement of heat transfer in ferrofluids with steady magnetic fields. Their problem was based on the flow between vertical parallel plates and in a box, which concluded that the heat transfer significantly increases with the influence of magnetic field gradient. Besides this, Kuncser*et al.* [6] and Li *et al.* [7]came up with the studies of the use of ferrofluids which aims to show the heat transfer enhancement in the boundary layer.Due tomany interesting applications of ferrofluids in industry including polymer technology, geophysics, solar physics and so on,many researchers performed the study of magnetohydrodynamics (MHD). Also for various novel interesting properties, ferrofluidsare used in many engineering applications including heat transfer, the magnetically controlled thermal flow, sealing technology, biomedicine, printer inks, magneto-rheological fluids and shock absorbers which are described in details in Popplewell [8].

Nadeem and Lee [9] studied the nanofluid flow over an exponentially stretching sheet while Khan and Pop [10] studied laminar boundary layer flow of nanofluid over a stretching sheet. Recently, Khan *et al.*[11] considered the problem of flow and heat transfer of ferrofluids past a plate with uniform heat flux and slip velocity. The effects of magnetic parameter, slip coefficient, the suction/injection parameter on the flow and heat transfer characteristics on nanofluid are investigated by Yazdi *et al.*[12]. Ramli*et al.*[13] studied the problem of MHD flow and heat transfer of ferrofluids over a moving flat plate with slip effect and uniform heat flux. However, the effect of radiation with velocity slip has not been investigated yet. Hence, the purpose of the present study is to analyze the effect of velocity slip in the presence of thermal radiation with suction on a steady two-dimensional flow of a ferrofluid over a flat plate. For this a homogeneous model is studied for the forced convective flow and heat transfer of ferrofluids. The effects of magnetic field, slip velocity, radiation, suction on the dimensionless velocity, temperature, skin friction coefficient and heat transfer rate are investigated for both Fe_3O_4 and TiO_2 in water and kerosene oil.

2.Mathematical Formulation

In this study forced convective boundary layer flow and heat transfer of water and kerosene-based ferrofluids over a stationary flat plate in a constant magnetic field $B(x)$ is considered. The flow is assumed to be steady, laminar, two-dimensional and incompressible, alsopreferred nanoparticles and the base fluids are assumed to be inthermal equilibrium.The hydrodynamic slip is assumed at the fluid-solid interface and the viscous dissipation is neglected in the analysis. Also, the ambient temperature is assumed to be constant in this study. The ferroparticles moments instantly orient along the magnetic field lines in the presence of magnetic field, and as soon as the magnetic field is removed, the particle moments are randomized quickly. The flow configuration is illustrated in Figure 1. The standard boundary layer equations for this problem can be written as follows:

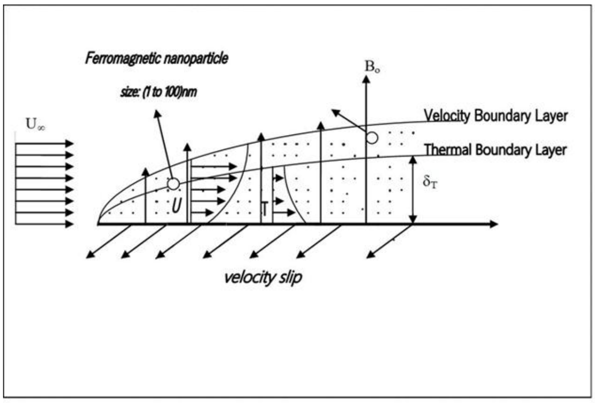

Figure 1. Schematic of the boundary layer flow over a flat plate.

$$\frac{\partial u}{\partial x}+\frac{\partial v}{\partial y}=0 \tag{1}$$

$$u\frac{\partial u}{\partial x}+v\frac{\partial u}{\partial y}=\nu_{nf}\frac{\partial^2 u}{\partial y^2}-\frac{\sigma B^2(x)}{\rho_{nf}}(u-U_\infty) \tag{2}$$

$$u\frac{\partial T}{\partial x}+v\frac{\partial T}{\partial y}=\alpha_{nf}\frac{\partial^2 T}{\partial y^2}-\frac{1}{\left(\rho C_p\right)_{nf}}\frac{\partial q_r}{\partial y} \tag{3}$$

subject to the boundary conditions,

$$\left.\begin{array}{llll} u=\gamma\frac{\partial u}{\partial y}, & v=v_w, & -\,k_{nf}\frac{\partial T}{\partial y}=q_w, & at\ y=0 \\ u\to U_\infty, & v\to 0, & T\to T_\infty, & at\, y\to\infty \end{array}\right\} \tag{4}$$

where, u and v are the velocity components along the x and y-axes, T is the temperature, ρ_{nf}, ν_{nf}, α_{nf} and $\left(C_p\right)_{nf}$ are the effective density, kinematic viscosity, thermal diffusivity and specific heat of the nanofluid respectively. σ and q_r are the electric conductivity and radiative heat flux respectively. γ is the slip parameter, U_∞ is the free stream velocity, v_w is the mass transfer, q_w is the wall heat flux and k_{nf} is the thermal conductivity of the nanofluid.

The transverse magnetic field is assumed to be a function of the distance from the origin defined as, $B(x)=B_0x^{-\frac{1}{2}}$ with $B_0\neq 0$, where x is the coordinate along the plate and B_0 is the magnetic field strength discussed by Khan *et al.* [11]. A permeable surface is considered with mass transfer velocity $v(x)$ as a function of x. Thus, $v_w=v_w^*x^{-\frac{1}{2}}$, $v_w^*\neq 0$. Due to suction $v_w(x)<0$ and $v_w(x)>0$ for injection Yazdi *et al.* [12].

The effective properties of ferrofluids may be expressed in terms of the properties of base fluid and ferroperticles and the volume fraction of solid ferroparticles as described in Khan *et al.* [11].

$$\left.\begin{array}{r} \nu_{nf}=\dfrac{\mu_{nf}}{\rho_{nf}}\,, \\ \mu_{nf}=\dfrac{\mu_f}{(1-\varphi)^{2.5}}\,, \\ \alpha_{nf}=\dfrac{k_{nf}}{\rho_{nf}\left(C_p\right)_{nf}}\,, \\ \rho_{nf}=(1-\varphi)\rho_f+\varphi\rho_s\,, \\ \left(\rho C_p\right)_{nf}=(1-\varphi)\left(\rho C_p\right)_f+\varphi\left(\rho C_p\right)_s\,, \\ \dfrac{k_{nf}}{k_f}=\dfrac{k_s+2k_f-2\varphi(k_f-k_s)}{k_s+2k_f+\varphi(k_f-k_s)}\,, \end{array}\right\} \tag{5}$$

where, φ is the volume fraction of solid ferroparticles and $\left(\rho C_p\right)_{nf}$ is the heat capacity of the nanofluid. Using the Rosseland [22] approximation as in Cortell [14], the radiative heat flux q_r in (3) is simplified as,

$$q_r = -\frac{4\sigma^*}{3k^*}\frac{\partial T^4}{\partial y}$$

where, k^* is the mean absorption coefficient and σ^* is the Stefen-Boltzman constant. We assume that the temperature differences within the flow region, namely, the term T^4 can be expressed as a linear function of temperature. The best linear approximation of T^4 is obtained by expanding it in a Taylor series about T_∞ and neglecting higher order terms. i.e. $T^4 = 4T_\infty^3 T - 3T_\infty^4$. Thus, equation (3) reduces to,

$$u\frac{\partial T}{\partial x} + v\frac{\partial T}{\partial y} = \alpha_{nf}\frac{\partial^2 T}{\partial y^2} + \frac{1}{(\rho C_p)_{nf}}\frac{16\sigma^*}{3k^*}T_\infty^3\frac{\partial^2 T}{\partial y^2} \tag{6}$$

The continuity equation (1) is satisfied if we choose a stream function Ψ, such that $u = \frac{\partial\Psi}{\partial y}$ and $v = -\frac{\partial\Psi}{\partial x}$. The similarity transformations are introduced as

$$\Psi = \nu_f\sqrt{Re_x}f(\eta)\ , \qquad \eta = \frac{y}{x}\sqrt{Re_x}\ , \qquad \theta(\eta) = \frac{T-T_\infty}{q_w x/k_f}\sqrt{Re_x}\ , \tag{7}$$

where, η is the similarity variable and $Re_x = \frac{U_\infty x}{\nu_f}$ is the local Reynolds number based on the free stream velocity and ν_f is the kinematic viscosity of the base fluid.Employing the similarity variables in equations (1)–(4), the following nonlinear system of ordinary differential equations are obtained

$$f''' + (1-\varphi)^{2.5}\left[\left(1-\varphi+\varphi\rho_s/\rho_f\right)\frac{1}{2}ff'' + M(1-f')\right] = 0, \tag{8}$$

$$\frac{k_{nf}/k_f}{1-\varphi+\varphi\left((\rho C_p)_s/(\rho C_p)_f\right)}\frac{1}{Pr}\left(1+\frac{4}{3}N\right)\theta'' + \frac{1}{2}\left(f\theta' - f'\theta\right) = 0, \tag{9}$$

subject to the boundary conditions,

$$\left.\begin{aligned} f(0) = f_w\,,\ f'(0) = \beta f''(0)\ ,\ \theta'(0) = -\frac{k_f}{k_{nf}}\ , \qquad & at\ \eta = 0 \\ f'(\eta) \to 1\ , \qquad \theta(\eta) \to 0\ , \qquad & as\ \eta \to \infty \end{aligned}\right\} \tag{10}$$

where, primes (') denote the differentiation with respect to η and $M = \frac{\sigma B_0^2}{\rho_f U_\infty}$ is the magnetic parameter , $N = \frac{4\sigma^*}{k_{nf}k^*}T_\infty^3$ is the radiation parameter , $Pr = \frac{(\mu C_p)_f}{k_f}$ is the Prandtl Number and $f_w = -\frac{2v_w^*}{\sqrt{\nu_f U_\infty}}$ is the suction parameter. We take $\gamma = c\sqrt{x}$, where c is a constant of dimension$L^{1/2}$ and obtain$\beta = c\sqrt{\frac{U_\infty}{\nu_f}}$ dimensionless slip parameter. The slip coefficient β is a dimensionless parameter ranging from zero (total adhesion) to infinity (full slip)as discussed by Yazdi*et al.*[12]. Thus, we have got four dimensionless parameters M, φ, N, Pr in the governing equations and two dimensionless parametersf_w, β in the boundary conditions.The physical quantities of interest are the skin friction coefficient C_f and the heat transfer rate at the surface, i.e. local Nusselt number Nu_x , which are defined as,

$$C_f = \frac{\tau_{wx}}{\rho_f U_\infty^2} \qquad (11) \qquad\qquad Nu_x = \frac{x q_w}{k_f (T_w - T_\infty)} \qquad (12)$$

where, τ_{wx} is the surface shear stress along the x-direction and q_w is the heat flux given by,

$$\tau_{wx} = \mu_{nf}\left(\frac{\partial u}{\partial y}\right)_{y=0} \text{ and } q_w = - k_{nf}\left(\frac{\partial T}{\partial y}\right)_{y=0}$$

Reduced dimensionless forms of (11) and (12) take the form, after fixing$Re_x = \frac{U_\infty x}{\nu_f}$,

$$Re_x^{1/2} C_f = \frac{f''(0)}{(1-\varphi)^{2.5}}. \qquad (13)$$

$$Re_x^{-1/2} Nu_x = \frac{1}{\theta(0)}. \qquad (14)$$

3.Keller-Box Method

Equations (8) and (9) subject to boundary conditions (10) are solved numerically using the implicit finite difference scheme called Keller-Box method as described by Na [15]and Cebeci and Bradshaw [16].

3.1 The Finite Difference Scheme

We introduce new dependent variables $u(x,\eta)$, $v(x,\eta)$ and $t(x,\eta)$ and $s(x,\eta)$ replaces $\theta(x,\eta)$ as the variable for temperature, with $f' = u, u' = v$ and$s' = t$, so that equations (8) and (9) become

$$v' + (1-\varphi)^{2.5}\left[\left(1 - \varphi + \varphi\, \rho_s/\rho_f\right)\frac{1}{2} f v + M(1-u)\right] = 0 \qquad (15)$$

$$\frac{(k_{nf}/k_f)}{\left[1-\varphi+\varphi((\rho C_p)_s/(\rho C_p)_f\right]}\frac{1}{Pr}\left(1+\frac{4}{3}N\right)t' + \frac{1}{2}(ft-us) = 0 \tag{16}$$

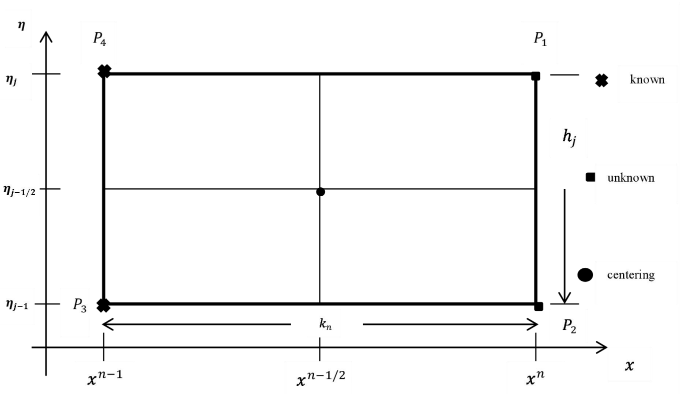

Figure 2. Net rectangle for difference approximation

Now, the net rectangle considered in the $x - \eta$ plane is shown in figure 2 and the net points are denoted by:

$$x^0 = 0, \quad x^n = x^{n-1} + k_n \qquad n = 1,2,\ldots\ldots\ldots\ldots,J$$

$$\eta_0 = 0,\ \eta_j = \eta_{j-1} + h_j \qquad j = 1,2,\ldots\ldots\ldots\ldots,J \qquad \eta_j = \eta_\infty$$

where, k_n is the Δx-spacing and h_j is the $\Delta\eta$-spacing. Here, n and j are just the sequences of numbers that indicate the coordinate location.The derivatives in the x-direction are replaced by finite difference, for example the finite difference for many points are,

(a) $\quad ()_j^{n-\frac{1}{2}} = \frac{1}{2}[(\ )_j^n + (\ )_j^{n-1}]\,, \quad ()_{j-\frac{1}{2}}^n = \frac{1}{2}[(\ )_j^n + (\ )_{j-1}^n]$

(b) $\quad \left(\frac{\partial u}{\partial x}\right)_{j-\frac{1}{2}}^{n-\frac{1}{2}} = \frac{u_{j-\frac{1}{2}}^n - u_{j-\frac{1}{2}}^{n-1}}{k_n}\,, \qquad \left(\frac{\partial u}{\partial \eta}\right)_{j-\frac{1}{2}}^{n-\frac{1}{2}} = \frac{(u)_j^{n-\frac{1}{2}} - (u)_{j-1}^{n-\frac{1}{2}}}{h_j}$

We will write the finite-difference form of equations for the midpoint $\left(x^n,\eta_{j-\frac{1}{2}}\right)$ of the segment P_1P_2 using centered difference derivatives. The process is called centering about $\left(x^n,\eta_{j-\frac{1}{2}}\right)$.In terms of new dependent variables, the boundary conditions become,

$$f(x,0) = f_w \quad u(x,0) = \beta v(x,0) \quad t(x,0) = -\frac{k_f}{k_{nf}} \\ u(x,\infty) = 1 \qquad s(x,\infty) = 0 \Bigg\} \tag{17}$$

The transformed boundary layer thickness η_j is sufficiently large so that it is beyond the edge of the boundary layer as described in Keller and Cebeci [17].The boundary conditions yield at $x = x^n$ are,

$$f_0^n = f_w \quad u_0^n = \beta v_0^n t_0^n = -\frac{k_f}{k_{nf}} \\ u_J^n = 1 \qquad s_J^n = 0 \Bigg\} \tag{18}$$

3.2 Newton's Method

To linearize the nonlinear system using Newton's method we introduce the following iterates.

$$\left.\begin{array}{c} f_j^{(i+1)} = f_j^{(i)} + \delta f_j^i \ , \quad u_j^{(i+1)} = u_j^{(i)} + \delta u_j^i , \\ v_j^{(i+1)} = v_j^{(i)} + \delta v_j^i \ , \quad s_j^{(i+1)} = s_j^{(i)} + \delta s_j^i , \\ t_j^{(i+1)} = t_j^{(i)} + \delta t_j^i , \end{array}\right\} \tag{19}$$

Substituting these expressions in the system of equation and then drop the quadratic and higher order terms in $\partial f_j^{(i)}, \partial u_j^{(i)}, \partial v_j^{(i)}, \partial s_j^{(i)}, \partial t_j^{(i)}$ this procedure yields atridiagonal system. In order to maintain the correct values in all the iterates, we will take,

$$\delta f_0 = 0, \delta u_0 = 0, \delta t_0 = 0, \delta u_J = 0, \delta s_J = 0.$$

3.3 The Block Tridiagonal Matrix

The linearized difference equations have a block tridiagonal structure consists of variables which consists of block matrices. In our case, the elements are defined as:

$$\boldsymbol{A\delta} = \boldsymbol{r} \tag{20}$$

where,

$$A = \begin{bmatrix} [A_1][C_1] \\ [B_2][A_2][C_2] \\ \ddots \\ \ddots \\ \ddots \\ [B_{J-1}][A_{J-1}][C_{J-1}] \\ [B_J][A_J] \end{bmatrix}, \qquad \delta = \begin{bmatrix} [\delta_1] \\ [\delta_2] \\ \vdots \\ [\delta_{J-1}] \\ [\delta_J] \end{bmatrix}, \qquad r = \begin{bmatrix} [r_1] \\ [r_2] \\ \vdots \\ [r_{J-1}] \\ [r_J] \end{bmatrix}$$

To solve Equation (20), we assume that A is nonsingular and it can be factored into,

$$\boldsymbol{A} = \boldsymbol{L}\boldsymbol{U} \tag{21}$$

where,

$$\boldsymbol{L} = \begin{bmatrix} [\alpha_1] & & & & & & \\ [B_2] & [\alpha_2] & & & & & \\ & [B_3] & [\alpha_3] & & & & \\ & & \ddots & \ddots & & & \\ & & & \ddots & \ddots & & \\ & & & & [B_{J-1}] & [\alpha_{J-1}] & \\ & & & & & [B_J] & [\alpha_J] \end{bmatrix} \qquad \boldsymbol{U} = \begin{bmatrix} [I] & [\Gamma_1] & & & & & \\ & [I] & [\Gamma_2] & & & & \\ & & [I] & [\Gamma_3] & & & \\ & & & \ddots & \ddots & & \\ & & & & \ddots & \ddots & \\ & & & & & [I] & [\Gamma_{J-1}] \\ & & & & & & [I] \end{bmatrix}$$

$[I]$ is the identity matrix of order 5 and $[\alpha_i]$ and $[\Gamma_i]$ are 5×5 matrices whose elements are determined by the following equations:

$$[\alpha_1] = [A_1] \tag{22}$$

$$[A_1][\Gamma_1] = [C_1] \tag{23}$$

$$[\alpha_j] = [A_j] - [B_j][\Gamma_{j-1}], \quad j = 2,3,\dots\dots,J \tag{24}$$

$$[\alpha_j][\Gamma_j] = [C_j], \qquad j = 2,3,\dots\dots\dots,J-1 \tag{25}$$

By substituting (21) into equation (20), we get

$$\boldsymbol{LU\delta} = \boldsymbol{r} \tag{26}$$

$$\boldsymbol{U\delta} = \boldsymbol{W} \tag{27}$$

$$\boldsymbol{LW} = \boldsymbol{r} \tag{28}$$

where,

$$\boldsymbol{W} = \begin{bmatrix} [W_1] \\ [W_2] \\ \vdots \\ [W_{J-1}] \\ [W_J] \end{bmatrix}$$

and $[W_j]$ are 5×1 column matrices. The elements **W** can be solved from equation (28)

$$[\alpha_1][W_1] = [r_1] \tag{29}$$

$$[\alpha_j][W_j] = [r_j] - [B_j][W_{j-1}], \quad 2 \le j \le J \tag{30}$$

The step, in which, Γ_j, α_j, and W_j are calculated, usually referred to as the *forward sweep.*When the elements of **W** are found, equation (27) then gives the solution of δ in the so called *backward sweep,* in which the elements are obtained by the following relations:

$$[\delta_J] = [W_J] \tag{31}$$

$$[\delta_j] = [W_j] - [\Gamma_j][\delta_{j+1}], \quad 1 \le j \le J-1 \tag{32}$$

Once the elements of $\boldsymbol{\delta}$ are found, equation (19) can be used to find the (i+1)th iteration in equation (21). These calculations are repeated until some convergence criterion is satisfied and calculations are stopped when,

$$\left|\delta v_0^{(i)}\right| < \varepsilon_1, \tag{33}$$

where $\varepsilon_1$is the tolerance and the value is taken 10^{-5} throughout the computation.

4.Results and Discussions

Described in the previous section the implicit finite difference scheme Keller-Box methodis programmed in MATLAB with a step size $\eta = 0.01$ which is used to solve the coupled system with equation (8) and (9), combined with (10) in the interval $0 \le \eta \le \eta_{max}$. Where η_{max} is the finite value of the similarity variable η for the far-field boundary conditions. For the asymptotic boundary conditions, the result converges for high values of the similarity variable, $\eta_{max} = 12$, for all values of the parameters involved. The values of Prandtl number for the base fluid, water and kerosene are taken 6.2 and 21 respectively. The effect of the volume fraction of solid ferroparticlesφ is studied in the range $0 \le \varphi \le 0.2$, where $\varphi = 0.0$ represents the pure fluid water or kerosene. We will consider $f_w > 0$ for suction and $f_w < 0$ for injection.

Table 1: Thermophysical properties of base fluids (water and kerosene) and magnetic nanoparticle ($\boldsymbol{Fe_3O_4}$) [11] and non-magnetic nanoparticle ($\boldsymbol{TiO_2}$)[18].

Physical properties	Base Fluids		Magnetic Nanoparticle (Fe_3O_4)	Non-Magnetic Nanoparticle (TiO_2)
	Water	Kerosene		
$\rho\ (kg/m^3)$	997	783	5180	4250
$C_p (J/kg.k)$	4179	2090	670	686.2
$k (W/m.k)$	0.613	0.15	9.7	8.9538

Table 2: Comparison of skin friction-coefficient for specific values of velocity slip $\boldsymbol{\beta}$ and magnetic parameters $\boldsymbol{M}$with $\boldsymbol{\varphi = 0, N = 0, f_w = 0}$.

β	M	Blassius [19]	Cortell [20]	Rahman [21]	Yazdi [12]	Khan [11]	Present Work (Fe_3O_4)	Present Work (TiO_2)
0	0	0.3321	0.33206	-	-	0.33206	0.33205	0.33205
-	1	-	-	1.0440	1.0440	1.04400	1.04479	1.0447
0.5	-	-	-	0.6987	0.6987	0.69872	0.6989	0.69897

Table 1 shows the thermophysical properties of the base fluids and solid nanoparticles. Table 2 confirms that the present results are found to be in good agreement with the existing literature. Table 3 shows the variation of skin friction coefficient and Nusselt number with volume fraction, magnetic field strength, velocity slip, radiation and suction. It shows that an increase in volume fraction of the ferroparticles and nanoparticles increases the skin friction coefficient and Nusselt number for both water and kerosene based fluids. It can be seen that the skin friction is minimum for pure fluids. As the volume fraction of solid nanoparticles increases, there is an increase in density with the nanoparticle volume fraction and it enhances skin friction coefficient. However, magnetic ferroparticles have higher skin friction coefficient than the non-magnetic particle and the difference becomes more evident as φincreases.We observe both skin friction coefficient and Nusselt number increases with the increase of magnetic parameter $M$for both water and kerosene based ferrofluid. Also we can see that with an increase in velocity slip parameterβ, the skin friction coefficient decreases but the Nusselt number increases. As the slip parameter increases, the flow resistance decreases and as a result skin friction decreases. In case of no slip, the Nusselt numbers are found to be lower and they increase with increasing slip parameter.Table 3 also shows that skin friction coefficient and Nusselt number increase as suction parameter f_w increases for both water and kerosene based Fe_3O_4 and TiO_2. However the table indicates that there is no effect of radiation parameter N on skin friction coefficient whereas the Nusselt number decreases with the increase of radiation parameter.It is important to note that Water-based ferrofluids have lower skin friction and Nusselt numbers than Kerosesne based ferrofluids. This is due to lower densities and higher Prandtl numbers of kerosene-based ferrofluid. We can also comment that the difference between the skin friction coefficient of water based Fe_3O_4 and TiO_2 is not significant in most of the cases. This is also true for kerosene based ferrofluids as well as for Nusselt numbers. This implied that the magnetic nanoparticle and the non-magnetic nanoparticle do not result in a significant difference while making ferrofluid.

Table 3: Effects of the dimensionless parameters on Skin-friction Coefficient (C_f) and Nusselt Number (Nu_x) for each mixture of Fe_3O_4 and TiO_2 with water and kerosene as base fluids

φ	M	β	N	f_w	C_f (Fe_3O_4)	C_f (TiO_2)	Nu_x (Fe_3O_4)	Nu_x (TiO_2)
Water-Based ($Pr = 6.2$)								
0.0	0.1	0.5	0.5	0.5	0.87276069	0.87276069	1.85839767	1.85839766
0.01					0.88688241	0.88503522	1.89027494	1.88812412
0.1					1.02545833	1.00599461	2.01573883	1.99314934
0.2					1.20641960	1.16498984	2.15774549	2.10999712
	0.0				0.72254323	0.67402061	2.05336571	2.00203894
	0.05				0.97024941	0.92540778	2.10908804	2.06019045
	0.1				1.20641961	1.16498985	2.15774549	2.10999713
	0.2				1.65273888	1.61751883	2.24107103	2.19505708
0.1	0.1	0.0			1.23114543	1.20322414	1.68403916	1.66147912
		0.5			1.02548333	1.00599461	2.01573883	1.99314935
		1.0			0.89770023	0.88339319	2.16173702	2.13901081
		2.0			0.75536945	0.74674607	2.29786633	2.27495334
		0.5	0.0		1.02545833	1.00599461	2.77765121	2.74584046
			0.5		1.02545833	1.00599461	2.01573883	1.99314934
			1.0		1.02545833	1.00599461	1.28477171	1.63533598
			2.0		1.02545833	1.00599461	1.28477171	1.27088856
0.2	0.2		0.5	0.0	1.35939527	1.35069073	1.65734965	1.63191401
				0.5	1.65273888	1.61751882	2.23700905	2.19505708
				1.0	1.95979621	1.89588898	2.89047612	2.83198104
				2.0	2.59686183	2.47224567	4.34668837	4.26059732

Kerosene- Based ($Pr = 21$)								
0.0	0.1	0.5	0.5	0.5	0.87276069	0.87276069	4.22993024	4.22993024
0.01					0.88969105	0.88733421	4.41871459	4.40681848
0.1					1.05476984	1.03027708	5.02681737	4.90573652
0.2					1.26817573	1.21662093	5.74319807	5.49570916
	0.0				0.79443369	0.73445928	5.61531593	5.36052915
	0.05				1.03680337	0.98127581	5.68348476	5.43311084
	0.1				1.26817573	1.21662093	5.74319807	5.49570916
	0.2				1.70597023	1.61751883	5.84874829	5.60413465
0.1	0.1	0.0			1.27321557	1.23806077	4.26914906	4.15471754
		0.5			1.05476983	1.03027708	5.02681737	4.90573651
		1.0			0.91929395	0.90124626	5.35185654	5.22748404
		2.0			0.76848069	0.75751472	5.65160422	5.52401829
		0.5	0.0		1.05476983	1.03027708	7.46853957	7.27818908
			0.5		1.05476983	1.03027708	5.02681737	4.90573652
			1.0		1.05476983	1.03027708	3.93939944	3.84808756
			2.0		1.05476983	1.03027708	2.89861146	2.83475441
0.2	0.2		0.5	0.0	1.37263715	1.36156227	3.22110808	3.13546928
				0.5	1.70597023	1.66147161	5.84874829	5.60413464
				1.0	2.05659176	1.97566169	9.04748889	8.60760099
				2.0	2.78599859	2.62783592	16.1710521	15.31263347

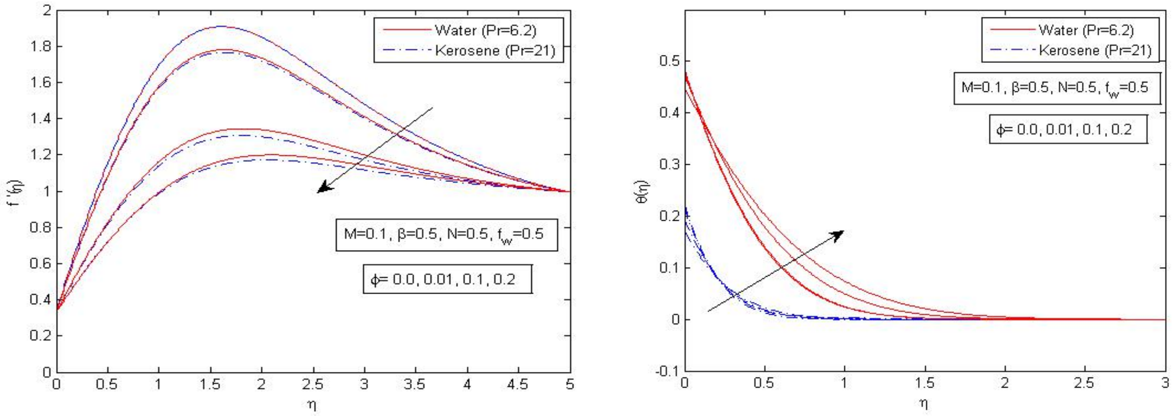

(a) (b)

Figure 3. Effects of volume fraction on dimensionless (a)velocity and (b) temperature profile for Fe_3O_4 for both water and kerosene based ferrofluids.

It is observed from Figure 3 (a) and 4 (a)that an increase in the volume fraction φ of the ferroparticle and nanoparticle pushes the fluid towards the plate surface as a result the fluid velocitydecreases. The effects of nanoparticle volume fraction on dimensionless temperature profiles are shown in figure 3 (b) and 4 (b). At first the thermal boundary layer decreases rapidly with increasing nanoparticle volume fraction. As φ increases, the thermal boundary layer thickness increases, leading to an increase in the plate surface temperature and thermal boundary layer thickness and a cross flow can be seen.

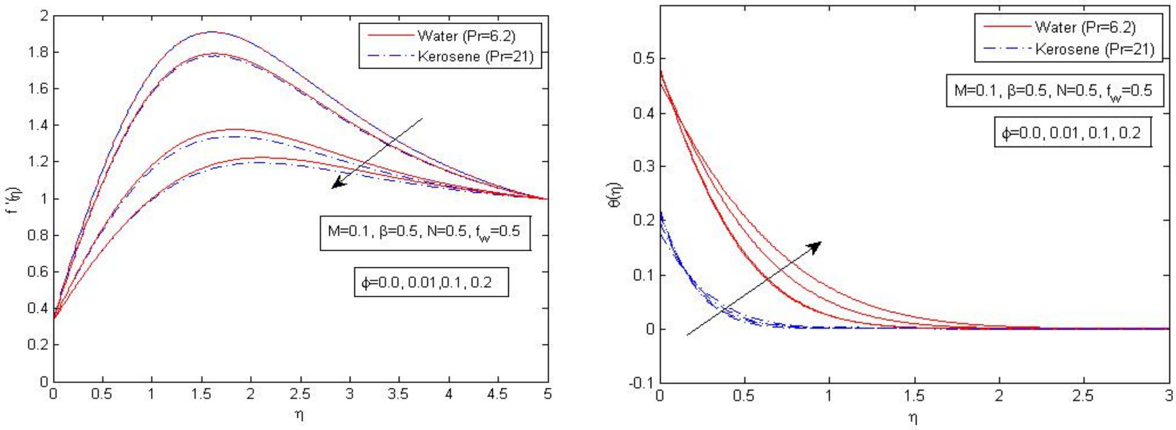

(a) (b)

Figure 4. Effects of volume fraction on dimensionless (a)velocity and (b) temperature profile for TiO_2 for both water and kerosene based nanofluids.

Fig 5 and Fig 6 show the effect of magnetic field parameter M on the convection. In the absence of magnetic field, the dimensionless velocity is found to be smaller. As the magnetic field is applied, it arranges the solid nanoparticles in the direction of magnetic field and enhances the dimensionless velocity.

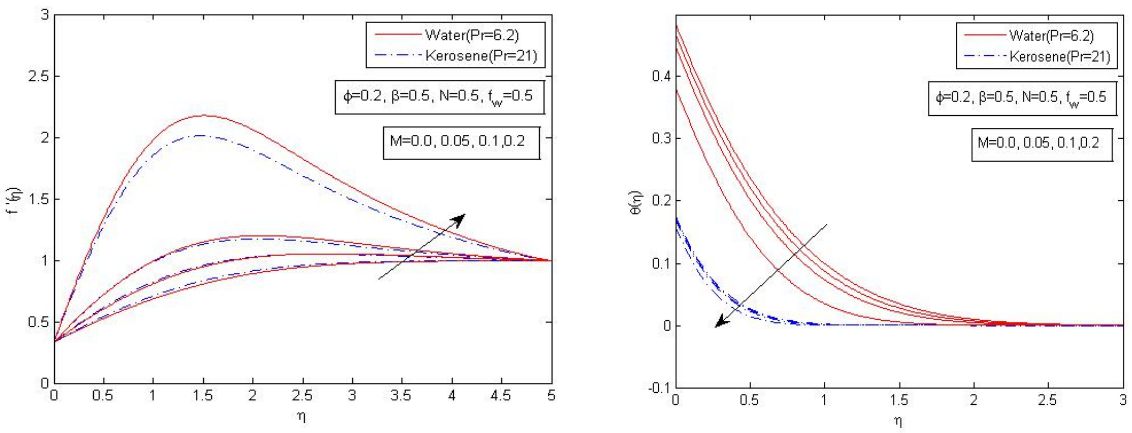

(a) (b)

Figure 5. Effects of magnetic parameter on dimensionless (a)velocity and (b) temperature profile for Fe_3O_4 for both water and kerosene based ferrofluids.

In Figure 5(a) and 6(a), it is observed that the velocity increases with increasing magnetic field intensity.The effects of magnetic parameter on dimensionless temperature are shown in figure 5(b) and 6(b). Due to increase in thermal conductivity with nanoparticle volume fraction the dimensionless surface temperature decreases with an increase in the magnetic parameter.It is also noticed that, due to the higher Prandtl number of kerosene, the thermal boundary layer thickness as well as the dimensionless surface temperature is small for each kerosene-based ferrofluid and nanofluid.

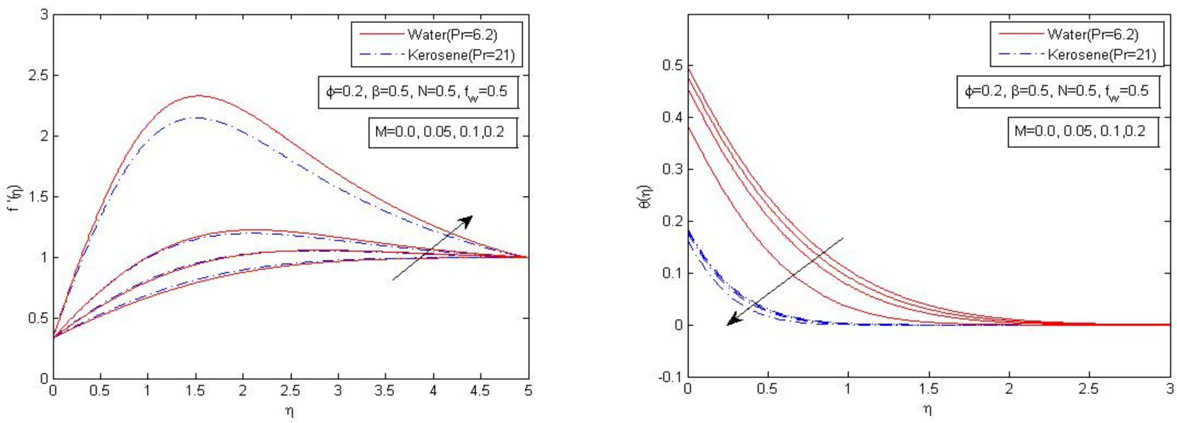

(a) (b)

Figure 6. Effects of magnetic parameter on dimensionless (a)velocity and (b) temperature profile for TiO_2 for both water and kerosene based nanofluids.

In Figure 7(a) and 8(a), it is observed that the velocity increases as slip parameter β increases. However, we observe a cross flow here. For non-zero β values, the velocity profiles increase with increasing β but after a certain point they start to decrease very rapidly with increase in β v and this produces a cross flow. The same characteristics is seen for kerosene based fluid.Figure 7(b) and 8(b) shows that an increase in slip parameter decreases the momentum boundary layer thickness as well as surface dimensionless temperature.

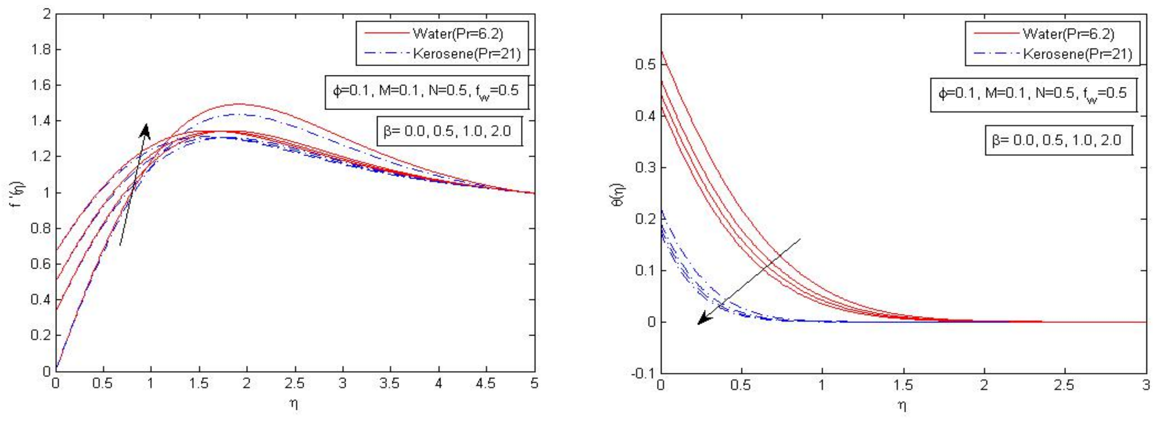

(a) (b)

Figure 7. Effects of dimensionless slip parameter on dimensionless (a)velocity and (b) temperature profile for Fe_3O_4 for both water and kerosene based ferrofluids.

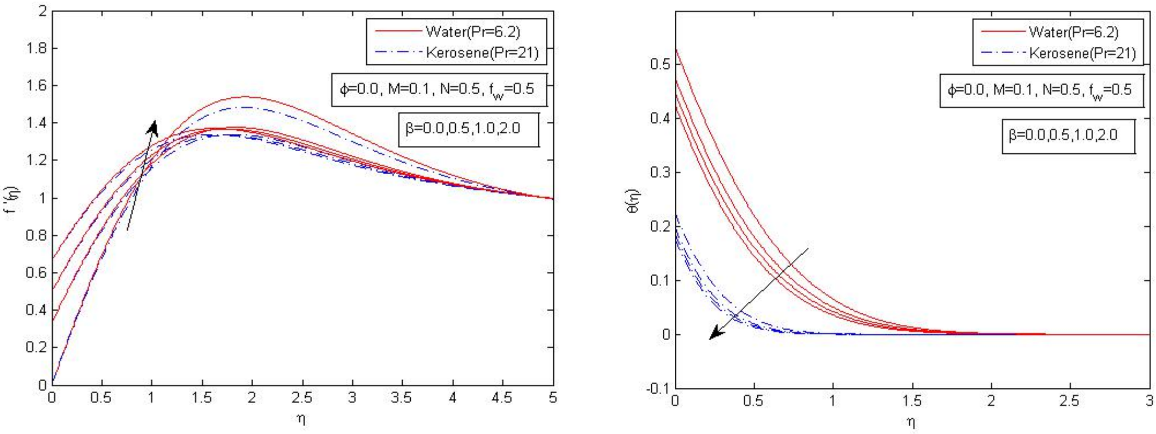

(a) (b)

Figure 8. Effects of magnetic parameter on dimensionless (a)velocity and (b) temperature profile for TiO_2 for both water and kerosene based nanofluids.

The effects of suction parameter f_w on velocity and temperature profiles are shown in Figure 9 and 10. It is observed in Figure 9 (a) and 10 (a) that an increase in suction parameter of the solid nanoparticle pushes the fluid towards the plate surface hence decreasing the fluid velocity. Since suction means more fluid is sucked out of the plate leading to a decrease in the thermal boundary layer thickness, figure 9(b) and 10(b) shows that an increase in suction parameter f_w results in decrease of temperature profiles.

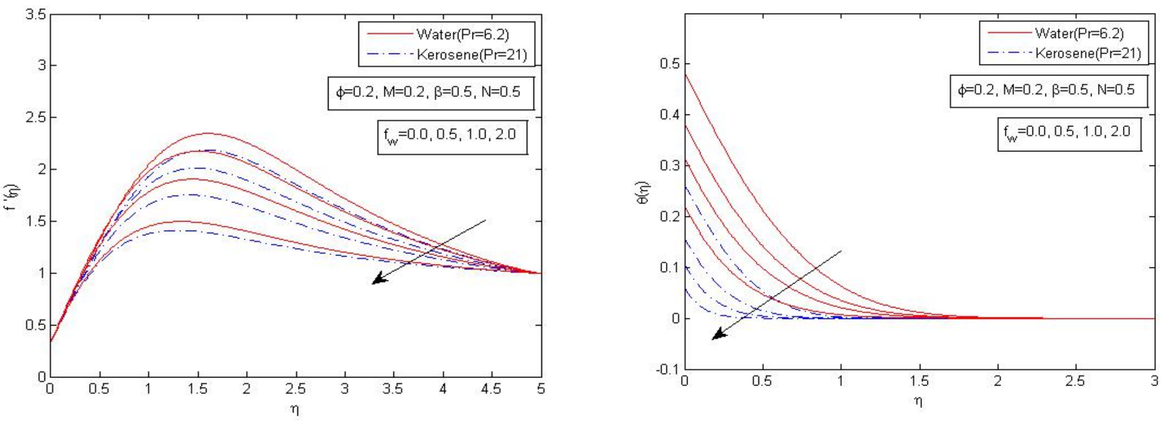

(a) (b)

Figure 9. Effects of suction parameter on dimensionless (a)velocity and (b) temperature profile for Fe_3O_4 for both water and kerosene based ferrofluids.

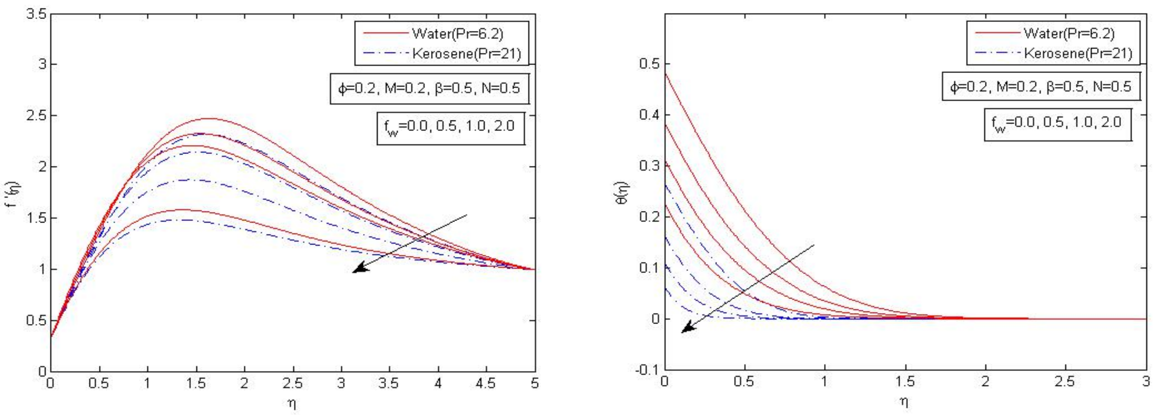

(a) (b)

Figure 10. Effects of suction parameter on dimensionless (a)velocity and (b) temperature profile for TiO_2 for both water and kerosene based nanofluids.

Since, skin friction remains unchanged with the increase in radiation parameter, the influences of radiation parameter on dimensionless velocity is not significant.

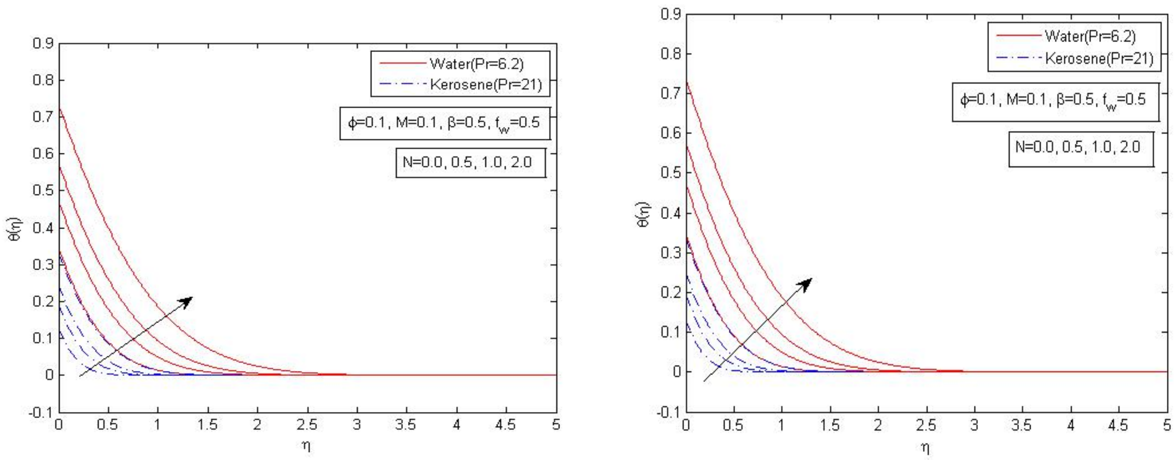

(a) (b)

Figure 11. Effects of radiation parameter on dimensionless temperature profile for both water and kerosene based fluids with (a) Fe_3O_4 and (b) TiO_2.

The effect of the radiation parameter N on dimensionless surface temperature is shown in figure 11 (a),(b). Larger amount of radiative heat energy is poured into the flow field indicate larger values of N causing rise in surface temperature. We conclude from the figure that increase in radiation parameter results in an increase in fluid temperature.

5.Conclusions

For both magnetite (Fe_3O_4) and titania $(TiO_2)$with water and kerosene as base fluids it can be concluded that :

- The skin friction coefficient increases with the increase of volume fraction, magnetic parameter, suction parameter.
- The skin friction coefficient decreases with increasingvelocity slip parameter.
- The skin friction coefficient has no effects on radiation parameter.
- Kerosene-based ferrofluids have higher skin friction and heat transfer rates than water based ferrofluids.
- Velocity profiles decrease with nanoparticle volume fraction and suction but increase with magnetic field and velocity slip.
- Radiation has no effect on the velocity profiles.
- Temperature profiles decrease with suction, magnetic field and velocity slip but increase with nanoparticle volume fraction and radiation.
- Due to the higher Prandtl number of kerosene, the momentum boundary layer thickness as well as the dimensionless surface temperatures is smaller for each kerosene based fluid.
- Water and kerosene based titaniaTiO_2 provides lower skin friction and heat transfer rates than water and kerosene based magnetite Fe_3O_4 but the difference implies that magnetic property of nanoparticles does not affect the characteristics significantly.
- With an increase in magnetic field strength the difference in skin friction and heat transfer rate of magnetic nanoparticles with TiO_2 decreases for both water and kerosene-based fluids.

Acknowledgements

Nomenclature		***Greek Symbols***	
B_0	Magnetic field intensity	α	Thermal diffusivity $[m^2/s]$
c_p	Specific heat $[J/Kg.K]$	β	Slip parameter
c_f	Skin friction coefficient	φ	Volume fraction of ferrofluid
f	Dimensionless stream function	η	Similarity variable

f_w	Suction parameter	μ	Absolute viscosity $[N.s/m^2]$
k	Thermal conductivity	ν	Kinematic viscosity $[m^2/s]$
M	Magnetic parameter	σ	Electric conductivity
N	Radiation parameter	ρ	Density $[kg/m^3]$
Nu_x	Local Nusselt number	ρc_p	Heat capacity $[kg/m^3 .K]$
Pr	Prandtl number of base fluid	θ	Dimensionless temperature
q_w	Wall heat flux $[W/m^2]$	Ψ	Stream function
q_r	Radiative heat flux $[W/m^2]$		
Re_x	Local Reynolds number		
T	Local fluid temperature $[K]$	***Subscripts***	
T_∞	Free stream temperature $[K]$	nf	Nanofluid
u	x-component of velocity $[m/s]$	f	Base fluid
U_∞	Free stream velocity $[m/s]$	s	Solid ferroparticles
v	y - component of velocity $[m/s]$	n,j	Sequence numbers that indicates
x	Distance along the plate $[m]$		$x-$ ηcoordinates.
y	Distance normal to the plate $[m]$		

References

[1] Choi, S.U.S., Enhancing thermal conductivity of fluids with nanoparticles,“ASME Publications”, vol.231/66, pp. 99-105, (1995).

[2] Xuan, Y., Li, Q., Heat transfer enhancement of nanofluids, “International Journal of heat and fluid flow”, vol. 21, pp. 58-64, (2000).

[3] Tiwari, R., Das, M., Heat transfer augmentation in a two-sided lid-driven differentially heated square cavity utilizing nanofluids, “Int. J. Heat Mass Transfer”,vol. 50, pp. 2002-2018, (2007).

[4] Ahmad, S., Rohni, A., Pop, I., Blasius and Sakiadis problems in nanouids, “ActaMech”., vol. 218, pp.195-204, (2011).

[5] Tangthieng, C., Finlayson, B., Maulbetsch, J., Cader, T., Heat transfer enhancement in ferrofluids subjected to steady magnetic fields,“J. Magn. n .Magn. Mater.”, vol. 201, pp.252-255, (1999).

[6] Kuncser, V., Schinteie, G., Sahoo, B., Keune, W., Bica, D., Vekas, L. and Filoti, G., Magnetic interactions in water based ferrouids studied by Mössbauer spectroscopy, "J. Phys. Condens. Matter.", 19(1), (2006).

[7] Li, M., Shi, H. and Zhu, L., Boundary layer velocity distribution of two special ferromagnetic fluid,"Proc. Eng.", vol.31, pp.166-169, (2012).

[8] Popplewell, J., Technological applications of ferrofluids, "Physics in technology", vol.15.3, pp.150, (1984).

[9] Nadeem, S., Lee, C., Boundary layer flow of a nanofluid over an exponentially stretching surface, "Nanoscale Res. Lett.", vol.7, pp.94, (2012).

[10] Khan, W. A., Pop, I., Boundary layer flow of a nanofluid past a stretching sheet, "Int. J. Heat Mass Transfer", vol.53, pp.2477–2483, (2010).

[11] Khan, W.A., Khan, Z.H. and Haq, R.U., Flow and heat transfer of ferrouids over a flat plate with uniform heat flux, "Eur. Phys. J. Plus.", 130(86), (2015).

[12] Yazdi, M., Abdullah, S., Hashim, I., Sopian, K., Effects of Viscous Dissipation on the Slip MHD Flow and Heat Transfer past a Permeable Surface with Convective Boundary Conditions, "Energies.", vol. 4, pp. 2273–2294, (2011).

[13] Ramli, N., Ahmed, S., Pop, I., Slip Effects on MHD Flow and Heat Transfer of Ferrofluids over a Moving Flat Plate, "AIP Conference Proceedings 1870", (2017).

[14] Cortell, R., Effect of viscous dissipation and radiation on the thermal boundary layer over a non-linearly stretching sheet, "PhysLett A.", vol. 372, pp. 631–636, (2008).

[15] Na, T. Y. Computational methods in Engineering Boundary value problem, "New York: Academic Press", (1979).

[16] Cebeci, T. and Bradshaw, P. Physical and Computational Aspects of Convective Heat Transfer,"New York:Springer", (1984).

[17] Keller, H.B., Cebeci, T., Accurate Numerical Methods for Boundary layer Flows,II: Two-Dimensional Turbulent Flows, "AIAA Journal.", 10:1193-1199, (1972).

[18] Oztop, H. F., Abu-Nada, E., Numerical study of natural convection in partially heated rectangular enclosures filled with nanofluids, "International Journal of Heat and Fluid Flow", vol. 29, 5, pp. 1326–1336, (2008).

[19] Blasius, H., Math, Z., Phys., vol. 56, 1, (1908).

[20] Cortell, R., Numerical solutions of the classical Blasius flat-plate problem, "Applied Mathematics and Computation", vol. 170, pp. 706–710, (2005).

[21] Rahman, M., Locally similar solutions for hydromagnetic and thermal slip flow boundary layers over a flat plate with variable fluid properties and convective surface boundary condition,“Meccanica.”,vol. 46, pp. 1127-1143, (2011).

[22] Rosseland S.Astrophysik und atom-theoretischeGrundlagen,“Berlin: Springer”, (1931).